ACS Synthetic Biology
Cite This: ACS Synth. Biol. 2019, 8, 1352−1360
Research Article
pubs.acs.org/synthbio

Intracellular Noise Level Determines Ratio Control Strategy Confined by Speed−Accuracy Trade-off

David Menn,[†] Patrick Sochor,[†] Hanah Goetz,[†] Xiao-Jun Tian,*[,†] and Xiao Wang*[,†]

[†]School of Biological and Health Systems Engineering, Arizona State University, Tempe, Arizona 85281, United States

Supporting Information

ABSTRACT: Robust and precise ratio control of heterogeneous phenotypes within an isogenic population is an essential task, especially in the development and differentiation of a large number of cells such as bacteria, sensory receptors, and blood cells. However, the mechanisms of such ratio control are poorly understood. Here, we employ experimental and mathematical techniques to understand the combined effects of signal induction and gene expression stochasticity on phenotypic multimodality. We identify two strategies to control phenotypic ratios from an initially homogeneous population, suitable roughly to high-noise and low-noise intracellular environments, and we show that both can be used to generate precise fractional differentiation. In noisy gene expression contexts, such as those found in bacteria, induction within the circuit's bistable region is enough to cause noise-induced bimodality within a feasible time frame. However, in less noisy contexts, such as tightly controlled eukaryotic systems, spontaneous state transitions are rare and hence bimodality needs to be induced with a controlled pulse of induction that falls outside the bistable region. Finally, we show that noise levels, system response time, and ratio tuning accuracy impose trade-offs and limitations on both ratio control strategies, which guide the selection of strategy alternatives.

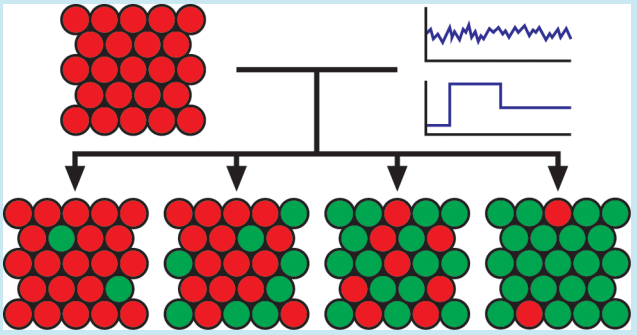

KEYWORDS: *synthetic biology, ratio tuning, stochasticity, fractional differentiation, cell fate*

Ratio control of differentiation within isogenic populations is a ubiquitous but poorly understood phenomenon. From single-celled microbes to higher organisms, many processes require mixed populations to carry out complex functions, such as bacterial persistence,[1,2] bacterial competence,[3,4] nasal and ocular receptor development,[5−7] differentiation of blood and vascular cells,[8] and immune response,[9] as well as stem cell maintenance and differentiation.[10] Several general explanations for how this phenotypic diversity arises have been proposed, such as stochastic fluctuations within gene regulatory networks,[11,12] asymmetrical sequestering of regulatory proteins during cell division,[13] and differential response to spatial gradients of extracellular soluble factors.[14] While each of these methods could theoretically generate a mixture of differentiated cells within a population, research has frequently focused on the types of cells yielded, rather than the quantitative control of their ratios. These processes are often tightly controlled in terms of ratio accuracy and attainment speed to avoid overspecialization or to ensure normal development.[15,16] Developing a unified understanding of the mechanisms and relevant factors to achieve and maintain precise ratio control will have widespread benefits in areas such as countering bacterial immunity,[17] treating diseases in which ratio control is disrupted, as is the case in some platelet disorders[18] or mastocytosis,[19] or in developing improved protocols for stem cell differentiation.[20,21]

As with many biological systems, the highly interconnected nature of the underlying genetic regulatory circuitry makes it difficult to study phenotypic ratio control without encountering myriad confounding variables. Synthetic biology, by cutting through to the basics of transcriptional regulation in isolated and orthogonal circuits, offers an attractive route for exploring mechanisms underlying ratio tuning.[22] Studying fundamental genetic motifs in isolation has yielded a greater understanding of key cellular behaviors, such as multistability, oscillation, and adaptation.[23−28] Multistable networks, specifically, are highly relevant for cellular differentiation processes and have wide applicability in a diverse range of contexts, from developmental biology[29] to targeted therapeutics[30] and cell-environment interactions.[31] Synthetic toggle switches have been implemented repeatedly in multiple organisms, demonstrating the feasibility of studying differentiation with minimal, synthetic circuits.[23,25,32,33] Further exploration of bistable circuits can reveal mechanisms of subpopulation control and manipulation, limitations of diverse control schema, and best practices for state transition control on single cell and population levels.[34,35] For example, recent work has studied how circuit component selection affects the network's hysteretic region[25] and how

Received: January 24, 2019
Published: May 14, 2019

DOI: 10.1021/acssynbio.9b00030
ACS Synth. Biol. 2019, 8, 1352−1360

inclusion of additional circuit components can be used to adjust population ratios.[36]

Here, we present methods for reliably tuning a multimodal population's ratios without the need for additional network components. First, using *E. coli*, we show that positioning a population with noisy intracellular expression dynamics within the bistable region can be enough to achieve fractional differentiation. Then, using the less noisy expression dynamics of *S. cerevisiae*, we demonstrate that temporary deviations from the bistable region can direct robust ratio differentiation in a low-noise system. By precisely modulating the stimulus strength and duration which moved the network toward the other state, we achieve reliable ratio tuning. From these findings, we develop a mathematical framework through which we can fully understand the roles of stimulus dosage, stimulus duration, and noise in driving fractional state switching of cellular populations. Gene expression noise acts as a global regulator of the speed and accuracy of ratio tuning, with noise level positively correlated with speed but negatively correlated with accuracy. Low noise systems become candidates for pulsed induction ratio tuning, in which an inverse correlation between stimulus dose and duration is observed, translating into a trade-off between the speed to attaining a chosen ratio and ratio accuracy.

RESULTS AND DISCUSSION

To investigate mechanisms of ratio control in bacteria, we first use the well-established bistable switch circuit.[37] The topology is that of mutual inhibition (Figure 1a) in which TetR and LacI repress one another while LacI is coexpressed with green fluorescent protein (GFP). TetR activity can be modulated with the addition of the small molecule anhydrotetracycline (ATc), which inhibits TetR activity and hence alleviates its inhibition on the expression of LacI. When grown in the absence of induction, the system favors the TetR dominant, low GFP state. A hysteresis curve was generated as a function of ATc concentration (Figure S1) to probe the cells' state distribution in and out of its bistable region. A fitting with a deterministic model indicated that the left bifurcation point is less than 0 ng/mL ATc, while the right bifurcation point is approximately 2 ng/mL ATc. Next, we developed a stochastic model (Table S1) for the system which shows strong agreement with the data (Figure 1b and Figure S2). Within the bistable region bimodal behavior was observed, with a portion of cells in the high GFP state while some were in the low GFP state (Figure 1c). This bimodality is believed to be caused by noise driven spontaneous state transitions.[4,38−41] Further long-term experiments and analyses were conducted to ensure the results were not affected by confounding factors (Figure S3).

To quantitatively understand the relationship between noise and the resulting bimodality of phenotypes, the stochastic model was used to explore the quasipotential landscape underlying this bistability. The quasipotential landscape is estimated by the probability distribution from the stochastic simulation of 1000 cells. It is shown that as ATc concentration increases, the depth of the left (low GFP) potential well decreases (Figure 1d). This essentially lowers the barrier of state transition from low GFP to high GFP, indicating that higher ATc induction would result in a larger percentage of cells in the high GFP state. Experiments indeed confirmed model predictions (Figure 1c, Figure S4a). It is noted that the main function of ATc is to stimulate the production of LacI by suppressing the inhibition of TetR on LacI and thus change the depth of the two steady states' quasipotential wells. Although ATc does not have a direct effect on the intracellular noise, it changes the amount of LacI and TetR, which determine the intracellular noise directly. This fraction changed little between measurements at 12 and 15 h, suggesting it is stable. Furthermore, it is shown that our model can predict such a ratio control with high quantitative accuracy (Figure 1e, Figure S4b,c), showing that high-GFP cell ratios increase monotonically but nonlinearly as ATc induction increases. Such a gradual and steady increase of ON cell percentage as a function of induction dosage could enable a precise ratio control for the entire bacterial population.

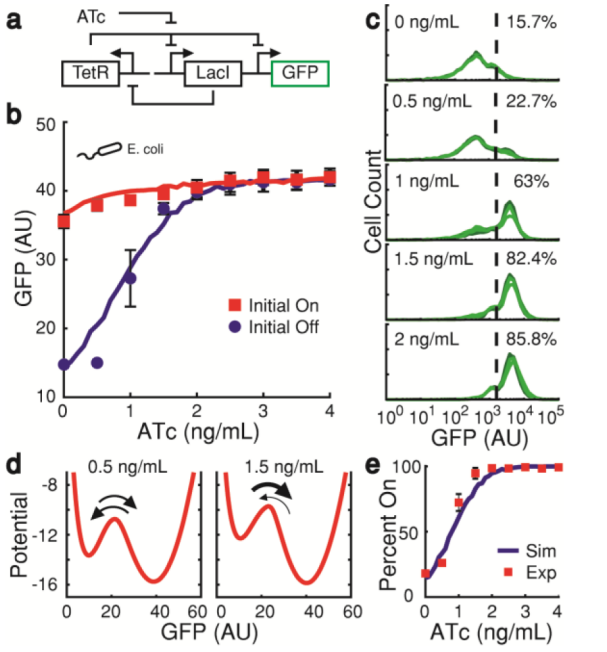

Figure 1. Gene expression noise in *E. coli* induces fractional differentiation within the bistable region. (a) Diagram of the mutual inhibition bistable switch. (b) In *E. coli*, this bistable switch exhibits hysteresis from 0 to roughly 1.5 ng/mL ATc. Within this range, cells can stably hold either the low GFP or high GFP states. The plot shows the mean of three replicates' medians ± SD, overlaid with model-predicted mean GFP values of 1000 simulated cells. Colored dots and squares are experimental results, and solid lines are simulation results. (c) Flow cytometry histograms of initially GFP-off populations show that as ATc dose increases, gene expression noise causes an increasing fraction of cells to spontaneously turn on. Dashed lines indicate an empirical threshold between OFF and ON cells. Three replicates are shown on each plot with corresponding dosage and the total percentage of ON cells noted. Data of 10 000 cells are collected for each experiment. (d) Quasi-potentials computed for different ATc dosages within the hysteretic region show the relative stability of the two steady states. At 0.5 ng/mL cells transition at similar rates between wells (arrows), but as ATc dosage increases to 1.5 ng/mL, the potential well for the low state becomes shallower, allowing cells to more easily transition to the high GFP state (represented by thicker arrowhead). Potential wells are generated from a stochastic simulation fit to the hysteresis curve data. (e) Stochastic model predicted ON percentage (blue line) fit experimental results (red square) accurately. The ON percentage is computed as the mean ON percentage of three replicates experimentally and that of 1000 simulated cells computationally for each dose of ATc.

DOI: 10.1021/acssynbio.9b00030
ACS Synth. Biol. 2019, 8, 1352−1360

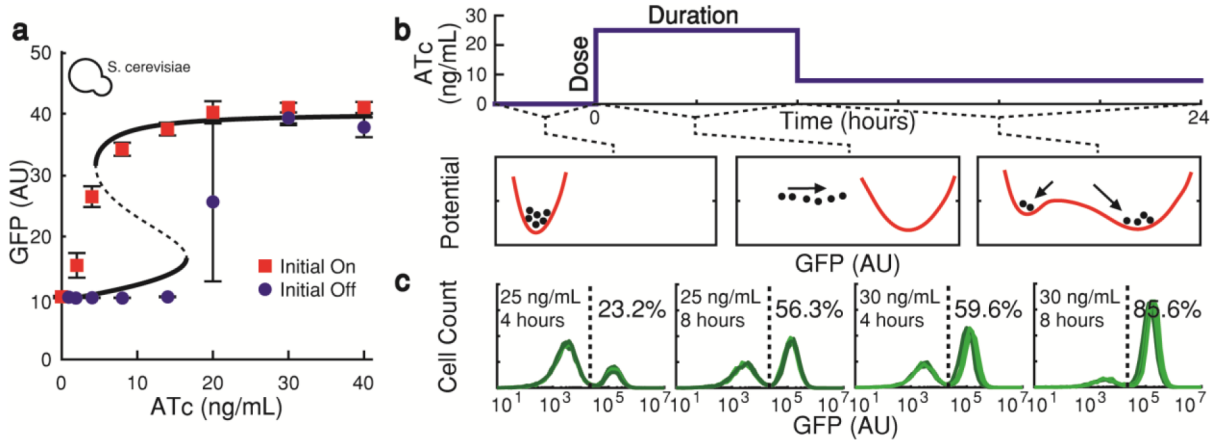

Figure 2. In *S. cerevisiae*, gene expression noise is lower, requiring temporary deviation from the bistable region to induce multimodality. (a) The hysteresis curve of the yeast toggle switch shows strong stability. The plot shows mean of three flow cytometry replicates' medians ± SD, overlaid with model-predicted hysteresis curve. (b) Yeast cells were exposed to pulses of ATc with varying dose and duration. Before the pulse (Phase I), all cells resided in the low-GFP state without any induction, corresponding to a single-welled potential landscape. The induction pulse (Phase 2) changes the underlying landscape to a single well in the high-GFP state, and cells begin to transition from low to high GFP state. Before all cells transition, induction is reduced to 8 ng/mL (Phase 3), at which there are two deep potential wells, low GFP and high GFP. Partially transitioned cells either transition fully or return to their initial low-GFP state. (c) Four flow cytometry experiments with four replicates each after pulse induction are shown with the total percentage of cells to the right of the dashed line. Inducer pulses for controlled durations allow for a wide range of ratios, with multiple paths to the same end point. Pulses of either 25 ng/mL or 30 ng/mL ATc for 4 or 8 h achieve a range of final ratios, with the 25 × 8 and 30 × 4 pulses producing nearly identical outcomes.

This finding of tunable ratio control by adjusting induction strength within the bistable region suggests one possible ratio control strategy for systems that require precise, but uncoordinated, fractional control of population differentiation. Bacteria, for example, could keep a subset of the colony in a dormant persister state to ensure survival in the case of unexpected environmental shifts or antibiotics.[1,2] Stochastic switching provides a simple mechanism for entering and exiting this state. A similar behavior is seen in the bacterial motility and adhesion decisions,[42,43] or in switching to a mutable, competent state.[15] In these cases, the overall ratio remains relatively fixed; though, individual cell's states are not. However, this strategy demands relatively high intracellular noise, which is common in plasmid-based bacterial systems,[44] so that individual cells could spontaneously transition between states within a reasonable amount of time.

Spontaneous and random back and forth switching between states is certainly not suitable for processes requiring irreversible cell fate determination, such as development and cell differentiation. In these contexts, the intracellular noise would need to be low enough to avoid spontaneous state switching. To identify possible ratio control strategies in such a low-noise environment, we transitioned experimentally to a less-noisy system: the chromosomally integrated mutual inhibition toggle in *S. cerevisiae*.[25] This circuit has the same topology as that shown in Figure 1a, exhibits hysteretic behavior (Figure 2a), and favors the TetR-dominant, low-GFP state under no induction. However, differences in promoters, copy number, and transcription−translation processes between *E. coli* and yeast serve to reduce intracellular noise and shift the bistable region up to roughly 3−17 ng/mL ATc. Unlike in *E. coli*, the bulk of the bistable range was impervious to the effects of intracellular noise, resulting in a single peak homogeneous expression profile even when the system is operating within the bistable region.[25] The noise level is set by the system's size Ω in Gillespie's stochastic simulation, which is widely used to control the noise in the gene regulator network.[45,46] Though noise does not determine the gene expression profile during the course of a typical experiment, if the stochastic simulation is run long enough, it indeed recapitulates the data well, as seen in Figure S5. Instead, to induce bimodality, we hypothesized that internal variability could be utilized by temporarily forcing the cells outside of the bistable region favoring another state. Then the population would begin to transition to the other state. However, natural stochasticity would cause some cells to transition faster than others. When the population was returned to the bistable region prior to full-population transition, some fraction of the cells would finish their transition while the rest would return to their original state. Figure 2b schematically illustrates this process and how the various stimulus levels adjust the underlying potential landscape to induce bimodality. This diagram also shows the two variables which determine population response: dose, which measures the magnitude of the induction pulse, and duration, the length of time for which the dose is applied. Using this method, the population achieved a specific phenotypic ratio and individual cells only transition between states once, which is distinct from *E. coli*.

Systematic temporal induction experiments were then designed and carried out to test our hypothesis. Using doses of 20, 25, 30, 35, and 40 ng/mL ATc, with pulse durations between 2 and 24 h, we comprehensively explored the range of ratios yielded by various dose/duration pairs (Figure S6). As seen in Figure 2c, there exists an inverse relationship between dose and duration, with increases in either variable causing a larger fraction of the population to transition to the high GFP state. Therefore, similar fractional responses can be obtained through multiple induction routes. For example, as demonstrated in the middle two panels of Figure 2c, 8 h of 25 ng/mL induction and 4 h of 30 ng/mL both produced about 59% of ON cells. Therefore, this pulsed induction method is experimentally verified to be able to produce tightly controlled yeast population ratios.

DOI: 10.1021/acssynbio.9b00030
ACS Synth. Biol. 2019, 8, 1352−1360

The model fit of the experimental data (Figure 3a) provides insight into the range of doses and durations appropriate for producing specific ratios. For example, with a 20 ng/mL ATc induction, it took between 18 and 24 h pulses to have greater than 70% of the cells to transition to the high GFP state, whereas a 40 ng/mL induction produced the same transition with a 4 h pulse. Generally, we observe that larger doses produce fast switching dynamics, and smaller doses required progressively longer durations to produce similar switch percentages. As evidenced by the very long durations for the 20 ng/mL dose, induction pulses near the bifurcation point could require durations of a day or more to cause a majority of cells to transition to high GFP, while ATc doses below 15 ng/mL have essentially no effect within the experimental time frame. With the use of experimentally validated model and parameters, more simulation data were analyzed to determine the robustness of the system to temporal perturbation of the pulse length. For this, we looked at the difference in time required to cause 30% and 70% of the population to transition, which we termed tuning range (TR = $T_{70} - T_{30}$). Figure 3b shows that while lower doses require longer durations to achieve a desired ratio (higher vertical positions of colored bars toward the left), these doses also have a bigger TR (longer vertical span of colored bars), suggesting that the ratio tuning in this region is more robust against temporal variation of induction pulses. For example, a 25 ng/mL dose generates 30% high GFP with a 4 h pulse and 70% with a 7 h pulse, resulting in a TR of 3 h. For 20 ng/mL induction, T_{30} and T_{70} both increase to 8 and 13 h, respectively, resulting in an overall larger TR of 5 h, indicating that there is more room for pulse-length error if a specific ratio within this range is desired. Conversely, larger doses, due to their fast switching dynamics, leave little room for error if a specific ratio is desired, with T_{30} and T_{70} being nearly the same. Results for on−off transitions show a similar relationship between induction dose and required duration (Figure S7), and *E. coli* exhibits similar, though noisier, switching behavior as well (Figure S8).

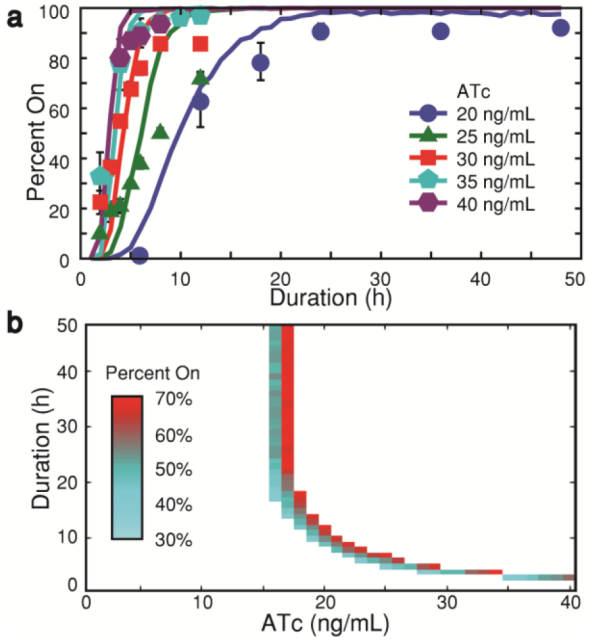

Figure 3. Mathematical modeling reveals the relationship between dose and duration needed for precise ratio control. (a) Experimental data (circles) were used to fit the stochastic model (lines) for multiple dose-duration pairs, showing strong agreement between the model and experimental results. Experimental data are the mean of four or five replicates' medians ± SD and the simulation data are the mean of 1000 simulated cells. (b) Further simulations show induction duration needed for a specific ratio increases exponentially as dose decreases until near the bifurcation point at roughly 20 ng/mL. Additionally, the tuning range from when a small portion of the population has switched states (teal) to when a large fraction has transitioned (red) is large at low doses but shrinks with increasing doses.

To develop a complete understanding of the relationship between noise and ratio control strategies across the noise spectrum, we employed an *in silico* approach that allows us to adjust the noisiness of gene expression while holding other system parameters constant. The model has been shown capable of recapitulating experimental results accurately under various conditions. It therefore serves as an appropriate tool to conduct thorough *in silico* explorations to meaningfully ratio control outcomes between high and low noise scenarios.

To investigate the effect of noise on system responsiveness to induction, simulations, like those shown in Figure S9, were carried out in low and high noise settings. Figure 4a shows that increasing noise reduces the time required for a population to transition to a new steady state ratio. The orange line indicates the steady state percentage of the population which will transition to the high-GFP state at a given ATc concentration. All distributions between 0 and 100% are represented within the circuit's bistable region, with the ATc concentrations resulting in 30% and 70% on cells (gray region) defining a region of broad tunability. The steady state is strictly 0 or 100% to the left or right of the bistable region, respectively. Because the time required to reach a steady state approaches infinity in the absence of noise, we measured the time needed for the population to reach half of the steady state ON percentage ($T_{halfmax}$). In the low noise setting (light blue line), $T_{halfmax}$ is very long within the bistable region, with times of 50 h or more for steady state ratios below 80%, suggesting it is almost experimentally impossible. This is consistent with our previous studies in yeast.[25] In the high noise setting (dark blue line), $T_{halfmax}$ is universally reduced. Beyond the bistable region, noise plays a less prominent role, with the high and low noise conditions resulting in almost identical transition times. These results indicate that constant induction within the bistable region is only a suitable ratio control strategy for systems with high enough noise to induce frequent and spontaneous state transitions, which is the case for *E. coli*.

Because of the long transition times in the low noise setting, the ratio control strategy for these cells becomes transient induction outside the bistable region. To compare the impacts of noise from multiple perspectives, we developed criteria to measure system responsiveness. Stimulus responsivity (SR = $1/T_{30}$) is a measure of the speed of transitions in response to a stimulus. A higher SR value means faster ratio control. Along with TR, both metrics can be calculated for pulsed inductions as used in Figure 2.

Both TR and SR were computed for simulations of pulsed inductions for various inducer concentrations in low noise (Figure 4b) and high noise (Figure S10) settings. Generally, noise causes a mild universal increase in SR, but differences in TR are only notable within the bistable region. As can be seen in Figure 4b, while the system's responsiveness (SR, red line) increases asymptotically as the dose increases, tolerance to error (TR, purple line) decreases. These data roughly divide

DOI: 10.1021/acssynbio.9b00030
ACS Synth. Biol. 2019, 8, 1352−1360

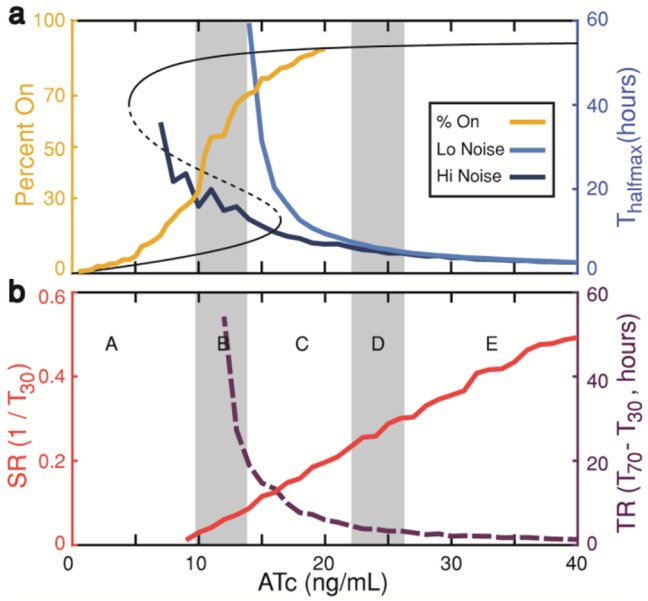

Figure 4. Gene expression noise determines appropriate method for achieving predictable ratio control. (a) High noise allows ratio control with constant induction. The orange line indicates the steady state population level average expression of the system, with the gray region bounded by constant induction dosage needed for 30% and 70% high GFP. Blue lines indicate $T_{halfmax}$ for low noise (light blue) and high noise (dark blue) environments. High gene expression noise reduces the time required for the population to transition from off to the steady state determined by inducer concentration. The hysteresis curve (black) is included for visual reference. (b) Low noise requires transient induction. Network transition speed (SR, red, left *y*-axis) and robustness (TR, dashed purple, right *y*-axis) of ratio control for a range of induction dosages. These curves divide the induction space into five regions. Regions A, C, and E are unsuitable for generating controlled ratios because cells do not transition (A), transition too slowly (C), or lack robust ratio control (E). Precise ratios can be attained in region B if noise is high enough to increase SR to an acceptable level. Region D is suitable for ratio control if both SR and TR are large enough, determined empirically. Here, region D meets the criteria SR > 0.25 and TR > 5 h in the low noise setting. $\Omega = 2$ for high noise and $\Omega = 10$ for low noise.

the system's induction range into five broad categories, labeled A−E. Regions A, C, and E are not suitable for either method of ratio control, but regions B and D (shaded gray) may be appropriate under certain conditions. Region A is unsuitable for ratio control because there is neither enough noise nor induction strength to cause a substantial fraction of the population to turn on. The boundaries of region B are fixed mathematically by the system's parameters and indicate the range of constant induction that could result in a broad range of precisely tuned ratios. However, as discussed, large enough intracellular noise is required to attain these ratios within a reasonably short time frame. Regions C−E cover induction levels only appropriate for pulsed induction, because constant induction at these levels will eventually cause most cells to turn on. The borders separating these three regions are determined by SR and TR: the C−D border set by SR, and D−E border set by TR. The location of these borders should vary between organisms and could be determined by the cell's physiological constraints and needs in their natural settings. Here, the constraints of SR > 0.25 and TR > 5 h provide a good inducer range D that balances speed and accuracy for the low noise condition. In region C, the system is highly tunable (large TR) but responds too slowly (small SR). In region E, the response time is fast (large SR), but tuning accuracy is lost (small TR). Region D finds a compromise between SR and TR constraints and is therefore appropriate for pulsed induction ratio control. The borders of region B are fixed mathematically and are suitable for constant induction ratio control. Those of region D are softer and produce tightly controlled ratios via pulsed induction. These borders are limited more by experimental constraints, and those shown in Figure 4 demonstrate the inherent trade-off between speed and accuracy.

In this work, we have used the mutual inhibition toggle switch—a synthetic version of a common genetic memory motif—to explore the temporal aspects of cell fate determination. Extracellular factors can drive a fraction of a population to switch phenotype and these factors interplay with intracellular gene regulation networks and noise to determine population response. In the case of *E. coli*, with noisy gene expression dynamics, applying constant induction within the bistable region was enough to elicit state-switching. With the less noisy kinetics observed in *S. cerevisiae*, on the other hand, cells retained their steady state behavior unless temporarily forced out of the bistable region with a pulse of induction. Through both methods, it was demonstrated that control of population ratios could be achieved with a high degree of precision.

In the case of transiently introduced pulses of extracellular factors, we show that there exists an inverse relationship between the strength of the stimulus and duration for which it is needed. A target ratio can be achieved reliably either with a strong pulse for a short duration or vice versa. Under this framework, the only limitation for achieving precise ratio control is the temporal resolution imposed by the physical constraints in removing cells from the forcing stimulus. We also observed a trade-off between system response speed and tuning robustness, quantified in the concepts of SR and TR. Lower pulse doses tended to be more robust to temporal variation in pulse length but required long durations to reach a desired ratio, while the opposite was true for high doses. This trade-off between speed and accuracy is found throughout intrinsically stochastic biological contexts.[47] Furthermore, gene expression noise acts as a global regulator of state switching. Increasing noise reduces transition times for both constant and pulsed inductions, increasing speed but resulting in a small reduction in tuning accuracy. Through this mechanism, noise levels determine whether constant induction will cause transitions within a reasonable time and determine the final dose at which pulsed induction should be set. Intracellular noise, therefore, is integral for the choice of ratio control strategy as well as for the chosen strategy's implementation.

In addition to the specific network studied, we also introduce a framework to analyze complex cellular behaviors involving a temporal component. Timing of cellular processes is becoming an increasingly important area of study,[48,49] and analogies can be drawn to applied fields of study. Though significantly more complex, the methods for deriving specific phenotypes from pluripotent progenitors are similar to the method we employ here.[20,21] Pluripotent cells are grown in a cocktail of growth factors for specific periods of time, sometimes sequentially, to force differentiation down a desired path. While this work has been biologically and empirically driven in the past, we suggest that a mathematical approach may yield further insight into directed differentiation methods.

DOI: 10.1021/acssynbio.9b00030
ACS Synth. Biol. 2019, 8, 1352−1360

Additionally, we compared ratio tuning strategies between organisms, showing that response times and noise profiles differed vastly between *E. coli* and *S. cerevisiae*. Because these model organisms are often used to draw inferences about gene networks more generally, understanding the nuances of their behavior and how they differ from other cell types, like mammalian systems, is important. Adjusting noise profiles *in silico* is a useful tool,[50−53] but it is no substitute for studying the phenomenon in living systems.[54−56] By better understanding how noise is manifest in natural circuits, we will be better able to devise strategies to utilize and control noise to make more reliable gene networks.[57−59]

Through this work we have shown the importance of considering the temporal evolution and expression noise of a system when analyzing its differentiation dynamics. We developed and leveraged a mathematical understanding of the bistable toggle switch to achieve robust control of fractional differentiation ratios. Further work along these lines could have wide-ranging applications in countering bacterial persistence, developmental or stem cell biology, therapeutics, and provide guidance for *de novo* gene network synthesis.

METHODS

Plasmids and Cell Strains. *E. coli* experiments were performed with K12 MG1655 (American Type Culture Collection, ATCC, #700926) modified with (ΔLacI ΔAraC) deletions. The toggle switch plasmid, pKDL, was provided generously as a gift from James Collins.[37] All yeast experiments were performed in YPH500 cells (Stratagene). The genomically integrated toggle system was developed previously by our group in collaboration with James Collins.[25]

Flow Cytometry and Data Analysis. All cell measurements were taken with a Becton Dickinson (BD) Accuri C6 flow cytometer. Front scatter (FSC-A) and side scatter (SSC-A) were used to gate cellular populations. Only a very course gating was used which removed debris smaller than the cell size but maintained the full range of population size variation. Samples were run on high flow rate to 10 000 captured events. The FL-1 channel (488 nm excitation; 530 ± 15 nm filter) was used to measure GFP fluorescence. Data were analyzed using MATLAB (Mathworks, Inc.) run on a personal computer.

***E. coli* Experiments.** The pKDL toggle switch was transformed into the *E. coli* using a transformation kit (Zymo Research) and selected for by plating on Luria Broth (LB) agar (Sigma-Aldrich) plates with added kanamycin (Sigma-Aldrich). Cells were picked the day prior to performing experiments and cultured in 5 mL of LB medium (Sigma-Aldrich) with kanamycin (Sigma-Aldrich). The following day, cell density was measured with flow cytometry and diluted to 1.5 cells/μL in fresh LB media with kanamycin.

For hysteresis experiments, after 2 h, cells were rediluted into medium with anhydrotetracycline (ATc; Sigma-Aldrich) forcing them to the initial off (ATc = 0; the cells favored the off state after overnight growth) or initial on (ATc = 20 ng/mL) states. These were maintained with hourly dilutions for 3 h, then rediluted in medium containing variable ATc levels (0, 0.5, 1, 1.5, 2, 2.5, 3, 3.5, and 4 ng/mL). When diluting from a high ATc concentration to a lower one, media volumes of different concentrations were mixed to avoid the potential shock of centrifugation and washing. For example, to go from 20 ng/mL to 4 ng/mL ATc, 1 part of the original culture was added to 4 parts at 0 ng/mL, yielding a final concentration of 4 ng/mL. To dilute from initial on to 0 ng/mL, cells were centrifuged and washed with fresh LB before redilution. The cultures were rediluted in fresh medium to 1.5 cell/μL every 3 h to avoid overgrowth and monitor healthy growth. They were measured every 3 h until they had achieved steady state expression at 15 h.

For dose/duration experiments (Figure S8), cells were again forced to their initial state for 3 h, then rediluted with medium containing the desired dose of ATc. At each time point, a portion of the culture was run on flow cytometry and another portion was rediluted to within the toggle's bistable range (0.125 ng/mL) using a similar fractional volume method of increasing or decreasing the concentration. The longest pulse given was 4 h, and all cultures were maintained with hourly dilutions. All cultures were tested via flow cytometry 4 h after the beginning of the pulse and again 1 h later to ensure that the population had reached steady state expression.

***S. cerevisiae* Experiments.** A single copy of the toggle switch was integrated into the yeast genome as described in a previous work.[25] Confirmed clones were streaked onto 2% glucose YPD agar plates (Sigma-Aldrich). Colonies were picked from these plates 42 h prior to the start of the experiment and grown in 5 mL of YPD medium. After 8 h, cultures were monitored by flow cytometry and rediluted to 1500 cells/mL in fresh YPD and allowed to grow overnight. After 12 h, cells were measured again and rediluted to 5000 cells/mL into yeast medium with 2% galactose (Sigma-Aldrich) and 1% raffinose (Sigma-Aldrich) with appropriate ATc to induce the initial off (0 ng/mL ATc) or initial on (50 ng/mL) states. These were measured and rediluted again 12 h later and allowed to grow overnight before the experiment was begun. For hysteresis experiments, initial off and initial on cells were diluted into varying concentrations of ATc (0, 0.5, 1, 2, 4, 8, 14, 20, 30, 40, 50 ng/mL). Cells were diluted to 5000 cells/mL every 12 h and measured via flow cytometry at 24 and 48 h. For dose/duration experiments, cultures were induced with ATc and at the end of each duration a portion of the culture was measured with flow cytometry and a portion was diluted down to an ATc concentration within the toggle's bistable range (8 ng/mL). Cells were measured and rediluted every 12 h after the start of the initial dose, with the final measure being at least 12 h after the end of the initial dose, to ensure that cells had reached steady state expression.

Modeling. We used the model proposed in previous work.[25] The ODEs are

$$[\mathrm{L}]' = \tau\left\{\mathrm{crl} + \frac{1.0}{1.0 + \left[\left(\frac{[T]}{k_t}\right)\left(1.0 + \frac{\mathrm{ATc}}{k_{\mathrm{atc}}}\frac{k_t}{[T]}\right)^{-m}\right]^{nt}}(\mathrm{cil} - \mathrm{crl}) - \mathrm{delta}[L]\right\} \quad (1)$$

$$[\mathrm{T}]' = \tau\left\{\mathrm{crt} + \frac{1.0}{1.0 + \left(\frac{[L]}{k_l}\right)^{nl}}\cdot(\mathrm{cit} - \mathrm{crt}) - \mathrm{delta}[T]\right\} \quad (2)$$

Where [L] and [T] are the concentration of LacI and TetR. LacI is coexpressed with GFP, and thus it was used interchangeably. crl and cil are the production rate of LacI when the promoter is repressed or induced, respectively, while

DOI: 10.1021/acssynbio.9b00030
ACS Synth. Biol. 2019, 8, 1352−1360

crt and cit are the production rate of TetR when the promoter is repressed or induced, respectively. k_t represents the active TetR concentration needed to make this probability 50%, and *nt* describes the nonlinearity of this inhibition. k_l represents the LacI concentration needed to make the promoter bound by LacI 50% of the time, and *nl* describes the nonlinearity of this inhibition. *m* is the Hill coefficient of the Hill function, which is used to describe the relationship between the active ratio of repressor TetR and the ATc inducer concentration. Here τ is the time scale of the system. The detail of the model construction can be found in our previous work.[25]

For the stochastic simulation, the concentration of each molecular species is converted to its number; that is, $x = [x]\Omega$, where Ω is a system size factor. Table S1 lists all the reactions involved. The τ-leap-based stochastic Gillespie algorithm is used for the stochastic simulation.[60,61] The noise level is set by Ω, which is set to 3 for *E. coli* system and 10 for *S. cerevisiae*. The quasi-potential landscape in Figure 1d and Figure 2b is defined as $U(x) = -\log(P_{ss}(X))$ where $P_{ss}(X)$ is the probability distribution from stochastic simulation with 1000 cells for 500 model hours. Figure 1d and Figure 2b show the resultant quasipotential landscape corresponding to a one-dimensional projection on the LacI axis. The bifurcation diagrams are generated with Oscill8 (http://oscill8.sourceforge.net/).

We searched the parameter space with a customized Metropolis algorithm (see the following section for details) to fit various experimental data, including the hysteresis curves (Figures 1b and 2a) and the fractions of the population to transition to the high GFP state (Figures 1e and 3a). It is noted that not all the parameters for *E. coli* and yeast are the same since we found different hysteresis curves in the two systems. It is an irreversible bistable switch in *E. coli* (Figure 1b), while it is a reversible bistable switch in *S. cerevisiae* (Figure 2a). To preserve the bistability for both systems and show the difference between them, we kept most of the parameters the same for the two systems as the synthetic circuit is topologically the same. We estimated the parameters based on our previous work[25] to make both systems bistable and then used the Metropolis algorithm to search the parameters that control the bistable ranges (including k_{act}, k_t, and k_l) and the time scale (τ) separately to fit various experimental data. The estimated and fitted parameters can be found in Table S2. In Figure 4, we used the parameters for *S. cerevisiae* under different noise levels to study the general strategies to achieve a predictable ratio.

Parameter Searching. The procedure for parameter searching with a customized Metropolis algorithm was as follows.

1. Choose a parameter set $\text{Para}_0 = [k_{act}, k_t, k_l, \tau]$ and calculate its fitting score, Score_0.
   a. For the *E. coli* system, for each ATc dose in the Figure 1b and 1e, the mean value of 1000 simulated cells will be calculated. Then the summation of the absolute values of the difference between the simulation data and experiments, i.e., mean absolute error (MAE), is calculated as the fitting score
   b. For the yeast system, for each ATc dose in Figure 2a and each ATc dose/duration combination point in Figure 3a, the mean value of 1000 simulated cells will be calculated. Then the summation of the absolute values of the difference between the simulation data and experiments, i.e., mean absolute error (MAE), is calculated as the fitting score. That is, $\text{score} = \frac{\sum |Y_{sim} - Y_{exp}|}{n}$, where Y_{sim} is the simulation results results and Y_{exp} is the experimental data.
2. Generate a new parameter set $\text{Para}_1 = \text{Para}_0(1 - \Delta P + \varepsilon 2\Delta P)$, where ΔP specifies the maximum percentage of change per step and ε is a vector of uniformly distributed random number in the interval (0,1).
3. Calculate the fitting score Score_1 with the parameter set Para_1.
4. Calculate the acceptance probability $p = e^{-(\text{Score}_1 - \text{Score}_0)/T}$. Generate a random number γ_1 from with uniform distribution between 0 and 1. Update $\text{Para}_0 = \text{Para}_1$ if $\gamma_1 < p$. Otherwise, reject the step k to $k + 1$.
5. Update the best score $\text{Score}_{best} = \min(\text{Score}_1, \text{Score}_0)$ and the corresponding best parameter set Para_{best}
6. Update step number k. If k is larger than a maximum step number, stop. Otherwise return to step 1.

■ ASSOCIATED CONTENT

Supporting Information

The Supporting Information is available free of charge on the ACS Publications website at DOI: 10.1021/acssynbio.9b00030.

Supplemental Figures S1−S10, expounding on experimental procedures and model fitting methods, and Tables S1−S2, detailing model construction and parameters (PDF)

■ AUTHOR INFORMATION

Corresponding Authors

*E-mail: xiaojun.tian@asu.edu.
*E-mail: xiaowang@asu.edu.

ORCID

Xiao-Jun Tian: 0000-0002-5601-2057
Xiao Wang: 0000-0002-4056-0155

Author Contributions

D.M., X-J.T., and X.W. designed the research. D.M. and P.S. performed experiments. X.-J.T. and H.G. developed computational models. D.M., X.-J.T., and X.W. analyzed the data and wrote the manuscript.

Notes

The authors declare no competing financial interest.

■ ACKNOWLEDGMENTS

D.M. and H.G. were supported by the Arizona State University Dean's Fellowship. This study was financially supported by an NIH grant (GM106081) (to X.W.) and the ASU School of Biological and Health Systems Engineering (X.-J.T.).

■ REFERENCES

(1) Balaban, N. Q., Merrin, J., Chait, R., Kowalik, L., and Leibler, S. (2004) Bacterial Persistence as a Phenotypic Switch. *Science 305* (5690), 1622−1625.
(2) Dhar, N., and McKinney, J. D. (2007) Microbial Phenotypic Heterogeneity and Antibiotic Tolerance. *Curr. Opin. Microbiol. 10* (1), 30−38.

DOI: 10.1021/acssynbio.9b00030
ACS Synth. Biol. 2019, 8, 1352−1360

(3) Gamba, P., Jonker, M. J., and Hamoen, L. W. (2015) A Novel Feedback Loop That Controls Bimodal Expression of Genetic Competence. *PLoS Genet. 11* (6), No. e1005047.
(4) Leisner, M., Kuhr, J.-T., Rädler, J. O., Frey, E., and Maier, B. (2009) Kinetics of Genetic Switching into the State of Bacterial Competence. *Biophys. J. 96* (3), 1178−1188.
(5) Bell, M. L., Earl, J. B., and Britt, S. G. (2007) Two Types of Drosophila R7 Photoreceptor Cells Are Arranged Randomly: A Model for Stochastic Cell-Fate Determination. *J. Comp. Neurol. 502*, 75−85.
(6) Mombaerts, P. (2004) Odorant Receptor Gene Choice in Olfactory Sensory Neurons: The One Receptor−One Neuron Hypothesis Revisited. *Curr. Opin. Neurobiol. 14* (1), 31−36.
(7) Wernet, M. F., Mazzoni, E. O., Çelik, A., Duncan, D. M., Duncan, I., and Desplan, C. (2006) Stochastic Spineless Expression Creates the Retinal Mosaic for Colour Vision. *Nature 440* (7081), 174−180.
(8) Potter, C. M. F., Lao, K. H., Zeng, L., and Xu, Q. (2014) Role of Biomechanical Forces in Stem Cell Vascular Lineage Differentiation. *Arterioscler., Thromb., Vasc. Biol. 34* (10), 2184−2190.
(9) Jeker, L. T., and Bluestone, J. A. (2013) MicroRNA Regulation of T-Cell Differentiation and Function. *Immunol. Rev. 253* (1), 65−81.
(10) Wu, J., and Tzanakakis, E. S. (2013) Deconstructing Stem Cell Population Heterogeneity: Single-Cell Analysis and Modeling Approaches. *Biotechnol. Adv. 31* (7), 1047−1062.
(11) Kærn, M., Elston, T. C., Blake, W. J., and Collins, J. J. (2005) Stochasticity in Gene Expression: From Theories to Phenotypes. *Nat. Rev. Genet. 6* (6), 451−464.
(12) Belete, M. K., and Balázsi, G. (2015) Optimality and Adaptation of Phenotypically Switching Cells in Fluctuating Environments. *Phys. Rev. E Stat. Nonlin. Soft Matter Phys. 92* (6), 062716.
(13) Wu, J., and Tzanakakis, E. S. (2012) Contribution of Stochastic Partitioning at Human Embryonic Stem Cell Division to NANOG Heterogeneity. *PLoS One 7* (11), e50715.
(14) Suslov, O. N., Kukekov, V. G., Ignatova, T. N., and Steindler, D. A. (2002) Neural Stem Cell Heterogeneity Demonstrated by Molecular Phenotyping of Clonal Neurospheres. *Proc. Natl. Acad. Sci. U. S. A. 99* (22), 14506−14511.
(15) Tang, L., Liu, R., Jin, G., Zhao, E., Liu, G., and Liu, S. (2014) Spontaneous Modulation of a Dynamic Balance between Bacterial Genomic Stability and Mutability: Roles and Molecular Mechanisms of the Genetic Switch. *Sci. China: Life Sci. 57* (3), 275−279.
(16) Pujadas, E., and Feinberg, A. P. (2012) Regulated Noise in the Epigenetic Landscape of Development and Disease. *Cell 148* (6), 1123−1131.
(17) Veening, J.-W., Stewart, E. J., Berngruber, T. W., Taddei, F., Kuipers, O. P., and Hamoen, L. W. (2008) Bet-Hedging and Epigenetic Inheritance in Bacterial Cell Development. *Proc. Natl. Acad. Sci. U. S. A. 105* (11), 4393−4398.
(18) Fialkow, P. J., Faguet, G. B., Jacobson, R. J., Vaidya, K., and Murphy, S. (1981) Evidence That Essential Thrombocythemia Is a Clonal Disorder with Origin in a Multipotent Stem Cell. *Blood 58* (5), 916−919.
(19) Hartmann, K., Bruns, S. B., and Henz, B. M. (2001) Mastocytosis: Review of Clinical and Experimental Aspects. *J. Invest. Dermatol. Symp. Proc. 6* (2), 143−147.
(20) Takahashi, K., Tanabe, K., Ohnuki, M., Narita, M., Ichisaka, T., Tomoda, K., and Yamanaka, S. (2007) Induction of Pluripotent Stem Cells from Adult Human Fibroblasts by Defined Factors. *Cell 131*, 861−872.
(21) Takahashi, K., and Yamanaka, S. (2016) A Decade of Transcription Factor-Mediated Reprogramming to Pluripotency. *Nat. Rev. Mol. Cell Biol. 17* (3), 183−193.
(22) Wang, L.-Z., Wu, F., Flores, K., Lai, Y.-C., and Wang, X. (2016) Build to Understand: Synthetic Approaches to Biology. *Integr. Biol. 8* (4), 394−408.
(23) Gardner, T. S., Cantor, C. R., and Collins, J. J. (2000) Construction of a Genetic Toggle Switch in Escherichia Coli. *Nature 403* (6767), 339−342.
(24) Stricker, J., Cookson, S., Bennett, M. R., Mather, W. H., Tsimring, L. S., and Hasty, J. (2008) A Fast, Robust and Tunable Synthetic Gene Oscillator. *Nature 456*, 516−519.
(25) Wu, M., Su, R.-Q., Li, X., Ellis, T., Lai, Y.-C., and Wang, X. (2013) Engineering of Regulated Stochastic Cell Fate Determination. *Proc. Natl. Acad. Sci. U. S. A. 110* (26), 10610−10615.
(26) Kim, J., Khetarpal, I., Sen, S., and Murray, R. M. (2014) Synthetic Circuit for Exact Adaptation and Fold-Change Detection. *Nucleic Acids Res. 42*, 6078.
(27) Wu, F., Su, R.-Q., Lai, Y.-C., and Wang, X. (2017) Engineering of a Synthetic Quadrastable Gene Network to Approach Waddington Landscape and Cell Fate Determination. *eLife 6*, No. e23702.
(28) Wu, F., Menn, D. J., and Wang, X. (2014) Quorum-Sensing Crosstalk-Driven Synthetic Circuits: From Unimodality to Trimodality. *Chem. Biol. 21* (12), 1629−1638.
(29) Chickarmane, V., Troein, C., Nuber, U. A., Sauro, H. M., and Peterson, C. (2006) Transcriptional Dynamics of the Embryonic Stem Cell Switch. *PLoS Comput. Biol. 2* (9), e123.
(30) Bu, P., Chen, K.-Y., Chen, J. H., Wang, L., Walters, J., Shin, Y. J., Goerger, J. P., Sun, J., Witherspoon, M., Rakhilin, N., et al. (2013) A MicroRNA MiR-34a-Regulated Bimodal Switch Targets Notch in Colon Cancer Stem Cells. *Cell Stem Cell 12* (5), 602−615.
(31) Oyarzún, D. A., and Chaves, M. (2015) Design of a Bistable Switch to Control Cellular Uptake. *J. R. Soc., Interface 12* (113), 20150618.
(32) Ausländer, S., and Fussenegger, M. (2013) From Gene Switches to Mammalian Designer Cells: Present and Future Prospects. *Trends Biotechnol. 31* (3), 155−168.
(33) Kramer, B. P., and Fussenegger, M. (2005) Hysteresis in a Synthetic Mammalian Gene Network. *Proc. Natl. Acad. Sci. U. S. A. 102* (27), 9517−9522.
(34) Menn, D. J., Su, R.-Q., and Wang, X. (2017) Control of Synthetic Gene Networks and Its Applications. *Quant. Biol. 5* (2), 124−135.
(35) Wang, L.-Z., Su, R.-Q., Huang, Z.-G., Wang, X., Wang, W.-X., Grebogi, C., and Lai, Y.-C. (2016) A Geometrical Approach to Control and Controllability of Nonlinear Dynamical Networks. *Nat. Commun. 7*, 11323.
(36) Ishimatsu, K., Hata, T., Mochizuki, A., Sekine, R., Yamamura, M., and Kiga, D. (2014) General Applicability of Synthetic Gene-Overexpression for Cell-Type Ratio Control via Reprogramming. *ACS Synth. Biol. 3* (9), 638−644.
(37) Litcofsky, K. D., Afeyan, R. B., Krom, R. J., Khalil, A. S., and Collins, J. J. (2012) Iterative Plug-and-Play Methodology for Constructing and Modifying Synthetic Gene Networks. *Nat. Methods 9* (11), 1077−1080.
(38) Maamar, H., Raj, A., and Dubnau, D. (2007) Noise in Gene Expression Determines Cell Fate in Bacillus Subtilis. *Science 317*, 526−529.
(39) Kim, K.-Y., and Wang, J. (2007) Potential Energy Landscape and Robustness of a Gene Regulatory Network: Toggle Switch. *PLoS Comput. Biol. 3* (3), No. e60.
(40) Acar, M., Becskei, A., and van Oudenaarden, A. (2005) Enhancement of Cellular Memory by Reducing Stochastic Transitions. *Nature 435* (7039), 228−232.
(41) Ozbudak, E. M., Thattai, M., Lim, H. N., Shraiman, B. I., and van Oudenaarden, A. (2004) Multistability in the Lactose Utilization Network of Escherichia Coli. *Nature 427* (6976), 737−740.
(42) Koirala, S., Mears, P., Sim, M., Golding, I., Chemla, Y. R., Aldridge, P. D., and Rao, C. V. (2014) A Nutrient-Tunable Bistable Switch Controls Motility in Salmonella Enterica Serovar Typhimurium. *mBio 5* (5), e01611−01614.
(43) Dressaire, C., Moreira, R. N., Barahona, S., Alves de Matos, A. P., and Arraiano, C. M. (2015) BolA Is a Transcriptional Switch That Turns off Motility and Turns on Biofilm Development. *mBio 6* (1), e02352−02314.

DOI: 10.1021/acssynbio.9b00030
ACS Synth. Biol. 2019, 8, 1352−1360

(44) Wong Ng, J., Chatenay, D., Robert, J., and Poirier, M. G. (2010) Plasmid Copy Number Noise in Monoclonal Populations of Bacteria. *Phys. Rev. E 81* (1), 011909 DOI: 10.1103/PhysRevE.81.011909.
(45) Thattai, M., and van Oudenaarden, A. (2001) Intrinsic Noise in Gene Regulatory Networks. *Proc. Natl. Acad. Sci. U. S. A. 98* (15), 8614−8619.
(46) Kar, S., Baumann, W. T., Paul, M. R., and Tyson, J. J. (2009) Exploring the Roles of Noise in the Eukaryotic Cell Cycle. *Proc. Natl. Acad. Sci. U. S. A. 106* (16), 6471−6476.
(47) Banerjee, K., Kolomeisky, A. B., and Igoshin, O. A. (2017) Elucidating Interplay of Speed and Accuracy in Biological Error Correction. *Proc. Natl. Acad. Sci. U. S. A. 114* (20), 5183−5188.
(48) Cheng, Y.-Y., Hirning, A. J., Josić, K., and Bennett, M. R. (2017) The Timing of Transcriptional Regulation in Synthetic Gene Circuits. *ACS Synth. Biol. 6* (11), 1996−2002.
(49) AkhavanAghdam, Z., Sinha, J., Tabbaa, O. P., and Hao, N. (2016) Dynamic Control of Gene Regulatory Logic by Seemingly Redundant Transcription Factors. *eLife 5*, 18458 DOI: 10.7554/eLife.18458.
(50) Faucon, P. C., Pardee, K., Kumar, R. M., Li, H., Loh, Y.-H., and Wang, X. (2014) Gene Networks of Fully Connected Triads with Complete Auto-Activation Enable Multistability and Stepwise Stochastic Transitions. *PLoS One 9* (7), No. e102873.
(51) Zhang, L., Radtke, K., Zheng, L., Cai, A. Q., Schilling, T. F., and Nie, Q. (2012) Noise Drives Sharpening of Gene Expression Boundaries in the Zebrafish Hindbrain. *Mol. Syst. Biol. 8*, 613.
(52) Chen, M., Wang, L., Liu, C. C., and Nie, Q. (2013) Noise Attenuation in the ON and OFF States of Biological Switches. *ACS Synth. Biol. 2* (10), 587−593.
(53) Wang, L., Xin, J., and Nie, Q. (2010) A Critical Quantity for Noise Attenuation in Feedback Systems. *PLoS Comput. Biol. 6* (4), e1000764.
(54) Ozbudak, E. M., Thattai, M., Kurtser, I., Grossman, A. D., and van Oudenaarden, A. (2002) Regulation of Noise in the Expression of a Single Gene. *Nat. Genet. 31*, 69−73.
(55) Blake, W. J., Balazsi, G., Kohanski, M. A., Isaacs, F. J., Murphy, K. F., Kuang, Y., Cantor, C. R., Walt, D. R., and Collins, J. J. (2006) Phenotypic Consequences of Promoter-Mediated Transcriptional Noise. *Mol. Cell 24*, 853−865.
(56) Kim, K. H., Choi, K., Bartley, B., and Sauro, H. M. (2015) Controlling E. Coli Gene Expression Noise. *IEEE Trans. Biomed. Circuits Syst. 9* (4), 497−504.
(57) Fu, W., Ergun, A., Lu, T., Hill, J. A., Haxhinasto, S., Fassett, M. S., Gazit, R., Adoro, S., Glimcher, L., Chan, S., et al. (2012) A Multiply Redundant Genetic Switch "locks in" the Transcriptional Signature of Regulatory T Cells. *Nat. Immunol. 13* (10), 972−980.
(58) Wu, F., Zhang, Q., and Wang, X. (2018) Design of Adjacent Transcriptional Regions to Tune Gene Expression and Facilitate Circuit Construction. *Cell Syst 6* (2), 206−215.
(59) Elowitz, M. B., Levine, A. J., Siggia, E. D., and Swain, P. S. (2002) Stochastic Gene Expression in a Single Cell. *Science 297* (5584), 1183−1186.
(60) Cao, Y., Gillespie, D. T., and Petzold, L. R. (2007) Adaptive Explicit-Implicit Tau-Leaping Method with Automatic Tau Selection. *J. Chem. Phys. 126* (22), 224101.
(61) Marquez-Lago, T. T., and Burrage, K. (2007) Binomial Tau-Leap Spatial Stochastic Simulation Algorithm for Applications in Chemical Kinetics. *J. Chem. Phys. 127* (10), 104101.

DOI: 10.1021/acssynbio.9b00030
ACS Synth. Biol. 2019, 8, 1352−1360